NJC

Accepted Manuscript

Volume 40 | Number 1 | January 2016 | Pages 1–846

NJC

New Journal of Chemistry
www.rsc.org/njc

A journal for new directions in chemistry

ISSN 1144-0546

ROYAL SOCIETY
OF CHEMISTRY

PAPER
Jason B. Benedict et al
The role of atropisomers on the photo-reactivity and fatigue of
diarylethene-based metal–organic frameworks

cnrs

This is an Accepted Manuscript, which has been through the Royal Society of Chemistry peer review process and has been accepted for publication.

Accepted Manuscripts are published online shortly after acceptance, before technical editing, formatting and proof reading. Using this free service, authors can make their results available to the community, in citable form, before we publish the edited article. We will replace this Accepted Manuscript with the edited and formatted Advance Article as soon as it is available.

You can find more information about Accepted Manuscripts in the author guidelines.

Please note that technical editing may introduce minor changes to the text and/or graphics, which may alter content. The journal's standard Terms & Conditions and the ethical guidelines, outlined in our author and reviewer resource centre, still apply. In no event shall the Royal Society of Chemistry be held responsible for any errors or omissions in this Accepted Manuscript or any consequences arising from the use of any information it contains.

ROYAL SOCIETY
OF CHEMISTRY

rsc.li/njc

ARTICLE

Pd anchored on C$_3$N$_4$ nanosheets/reduced graphene oxide: an efficient catalyst for the transfer hydrogenation of alkenes

Jie Li[‡], Saisai Cheng[‡], Tianxing Du, Ningzhao Shang*, Shutao Gao, Cheng Feng, Chun Wang*, Zhi Wang

College of Science, Hebei Agricultural University, Baoding 071001, China

In this work, porous g-C$_3$N$_4$ nanosheets/reduced graphene oxide (rGO) composite was synthesized *via* hydrothermal co-assembly of GO and g-C$_3$N$_4$ nanosheets (g-C$_3$N$_4$ NS). Compared with g-C$_3$N$_4$ NS, rGO and bulk g-C$_3$N$_4$/rGO, the g-C$_3$N$_4$ NS/rGO supported Pd nanocatalyst displayed a remarkable catalytic activity for the hydrogenation of alkene with formic acid and formates as hydrogen source at atmospheric pressure. Among all the as-prepared Pd-g-C$_3$N$_4$ NS/rGO catalysts, the optimized Pd-g-C$_3$N$_4$ NS/rGO$_{20}$ exhibited the highest turnover frequency of 133 mol mol^{-1} Pd h^{-1}, which is among the highest value reported in the documents. 99% of conversion and 99% of selectivity were achieved after 30 min reaction at 30 $^{\circ}$C for the hydrogenation of nitrobenzene. In addition, the Pd-g-C$_3$N$_4$ NS/rGO$_{20}$ exhibited an excellently high stability after five successive cycles without significant loss of its catalytic activity.

1. Introduction

Hydrogenation of unsaturated carbon-carbon bonds (C=C) is an important reaction in the chemical industry, particularly in the synthesis of flavor, fragrance chemistry and pharmaceuticals.[1] Generally, conventional process for alkene hydrogenation requires the use of pressurized molecular hydrogen (H$_2$) in combination with various metal catalysts.[2, 3] Although 100% conversion of alkene can be achieved using H$_2$, however, gaseous hydrogen is dangerous and difficult to handle due to its hazardous properties[4-6]. Therefore, from both sustainability[7, 8] and security perspective, exploring safer hydrogen sources for hydrogenation of unsaturated bonds is desirable[9-11].

Recently catalytic transfer hydrogenation (CTH) has been considered as a promising method for the hydrogenation of alkene, in which hydrogen is replaced by a hydrogen donor, such as formic acid[12], hydrazine, and isopropanol. In this case, the hydrogenation reaction can be performed under mild conditions (e.g. room temperature, atmospheric pressure), which represents a more cost-effective and greener approach[13-15]. Among the hydrogen donor employed in CTH, FA, a promising hydrogen source, has attracted

considerable interest in the area of sustainable chemistry due to its properties of high energy density, non-toxicity and excellent stability. FA has been used in transfer hydrogenation of nitro compounds,[1] fructose to g-valerolactone,[16] and alkene[17]. For example, Basset et al.[18] have developed palladium catalyst supported on fibrous silica nanospheres (KCC-1) for the hydrogenation of alkenes and α,β-unsaturated carbonyl compounds within 6-24 h at 100 $^{\circ}$C using of FA as hydrogen source. Du et al.[19] synthesized pyridine N-doped carbon immobilized Pd nanoparticles catalyst. The resulting catalyst Pd@CN exhibited enhanced efficiency and activity for alkene hydrogenation at 90 $^{\circ}$C within 12 h using FA as sustainable H$_2$ source. Zhao[17] fabricated Pd encapsulated triazine functionalized porous organic polymer catalyst and used for catalytic transfer hydrogenation of alkene in the presence of FA and Et$_3$N, the reactions were performed at 25 $^{\circ}$C for 4-15 h. Chen et al.[1] reported the application of g-C$_3$N$_4$ supported Pd nanoparticles (Pd/CN), a Mott-Schottky catalyst, in the hydrogenation of C=C compounds at room temperature. The reactions were conducted in an aqueous solution of formic acid within 3 h using 7.5 mol% Pd. Despite recent progress, the reported catalytic systems still have one or more shortcomings[20-22], such as harsh reaction conditions, long reaction time and high catalyst dosage.[23-25] Therefore, exploring highly active heterogeneous catalysts for the hydrogenation of alkene is still highly desirable[26, 27].

The graphite-like carbon nitride (g-C$_3$N$_4$) possesses many super physicochemical properties, such as nontoxic, excellent thermal and chemical stability, which make g-C$_3$N$_4$-based materials a new class of multifunctional nanoplatforms for electronic, catalytic and energy applications.[28, 29] Unfortunately, the performance of pristine g-C$_3$N$_4$ is restricted due to its small surface area and high recombination rate of electron-hole pairs. To address the problems, tremendous efforts

College of Sciences, Hebei Agricultural University, Baoding 071001, P. R. China.
Tel.: +86 312 7528291. E-mail: chunwang69@126.com;ningzhao611@126.com.
‡ : *These authors contributed equally to this work.*

ARTICLE

have been made to manipulate g-C$_3$N$_4$, such as designing an appropriate textural porosity,[30] metal oxide,[31-33] non-metal doping[34] and coupling with carbon materials.[12, 35, 36] Graphene, a 2-dimensional (2D) sp^2-conjugated carbon atoms packed in a honeycomb lattice, has received much attention because of its extraordinary chemical, physical and catalytic properties.[37-39] The coupling rGO with g-C$_3$N$_4$ may induce interesting synergetic effects.[40-42] In a recent work, Yong at al.[43] fabricated sandwich-like graphene/g-C$_3$N$_4$ (GCN) nanocomposites by urea and graphene oxide. The GCN demonstrated high visible-light photoactivity towards CO$_2$ reduction at ambient conditions, exhibiting a 2.3-fold enhancement over pure g-C$_3$N$_4$. Qu at al.[44] synthesized a three dimentional (3D) architecture composite with 1D g-C$_3$N$_4$ nanoribbons and 2D graphene by a simple one-step hydrothermal method. The catalyst exhibited efficient electrocatalytic ability for the hydrogen evolution reaction with low over potential and extremely large exchange current density. To the best of our knowledge, using graphene/g-C$_3$N$_4$ composite as catalyst or catalyst support for catalytic organic reaction still remains in their infancy. Liu[45] prepared uniform graphene/g-C$_3$N$_4$ composite, which provides efficient electron transfer interfaces to boost its catalytic oxidation activity for cycloalkane with relatively high yield, good selectivity, and reliable stability. Up to now, there has been no report on the use of the g-C$_3$N$_4$/rGO nanocomposite as supported catalyst for hydrogenation alkene reaction.

Herein, porous g-C$_3$N$_4$ nanosheets/reduced graphene oxide (rGO) composite was synthesized *via* hydrothermal co-assembly of GO and g-C$_3$N$_4$ nanosheets (g-C$_3$N$_4$ NS) (Scheme 1). The Pd nanoparticles were immobilized on g-C$_3$N$_4$ NS/rGO material by an impregnation method, which was employed to catalyze the transfer hydrogenation of alkenes with HCOOH and ammonium formate as hydrogen donor for the first time. The as-prepared Pd-g-C$_3$N$_4$ NS/rGO$_{20}$ displays excellent catalytic properties, including high catalytic activity and reliable stability, which is superior to the commercial Pd-C hybrids.

Scheme 1 Schematic illustration of the preparation process of the Pd-g-C$_3$N$_4$ NS/rGO catalyst.

2. Experimentals

2.1 Chemicals

Melamine, dichloromethane (CH$_2$Cl$_2$), rGO and GO, formic acid (HCOOH, 88%), ammonium formate (HCOONH$_4$), methanol, ethanol，concentrated sulfuric acid (H$_2$SO$_4$, 98%), anhydrous magnesium sulfate (MgSO$_4$), ammonium hydroxide (NH$_3$·H$_2$O, 25%) and sodium borohydride (NaBH$_4$, 96%) were purchased from Huaxin Co., Ltd (Baoding, China). Palladium chloride (PdCl$_2$, AR), 2-methylfurane (C$_5$H$_6$O, 99%), furfuryl alcohol (C$_4$H$_3$CH$_2$OH, 98%) and all of the alkenes compounds were obtained from Aladdin Chemicals Co Ltd. (Shanghai, China).

2.2 Characterization

The Brunauer-Emmett-Teller (BET) surface areas were determined from the N$_2$ adsorption at 77 K using V-Sorb 2800P (Jinaipu, China). The X-ray diffraction (XRD) patterns of the samples were recorded with a Rigaku D/max 2500 X-ray diffractometer (Dandong, China) using Cu *K*α radiation (30 kV, 25 mA) in the range 2θ = 2°-80°. The X-ray photoelectron spectroscopy (XPS) measurements were performed on an ESCA Lab 250 (Thermo) spectrometer (Shanghai, China) with a monochromatic Al *K*α source (1486.6 eV). A Hitachi S4800 field emission electron microscope (SEM, Tokyo, Japan) operated at 30 kV and transmission electron microscopy (TEM) using a JEOL model JEM-2011 (Tokyo, Japan) at 200 kV were used for determining the morphology of the samples. The Pd loading in the materials was analyzed by a T. J. A. ICP-9000 type inductively coupled plasma atomic emission spectroscopy (ICP-AES) instrument. The FTIR spectra were recorded using a Bruker IFS 66v/S FTIR spectrometer. GC analyses were carried out on an Agilent 7820A series gas chromatograph (Agilent Technologies, CA, USA) equipped with a flame ionization detector (FID) and a split/splitless injector. All the separations were performed on a HP-5 capillary column (30 m × 0.32 mm i.d. × 0.25 μm film thickness) (Agilent J&W Scientific, CA, USA).

2.3 Catalyst preparation

Synthesis of bulk g-C$_3$N$_4$ and g-C$_3$N$_4$ NS

Tapically, 5 g melamine was transferred to an alumina crucible covered with a lid and heated at 550 ^{o}C for 4 h at a ramp rate of 2.3 ^{o}C min^{-1}.[46] A yellowish solid was obtained (bulk g-C$_3$N$_4$), and was grinded to powders. g-C$_3$N$_4$ NS was synthesized via the chemical oxidation of bulk g-C$_3$N$_4$ with concentrated H$_2$SO$_4$.[47] The obtained g-C$_3$N$_4$ powers were dispersed in concentrated H$_2$SO$_4$ at a concentration of 300 mg·mL^{-1} at 100 ^{o}C for 2 h. Then the yellow liquid was slowly poured into 100 mL of deionized water and ultrasonicated for 1 h for exfoliation. The temperature of the suspension increased rapidly, and the mixture color changed from yellow to milk-white. Then, the obtained suspension was subjected to 10 min of centrifugation at 3000 rpm to remove any unexfoliated g-C$_3$N$_4$. After centrifugation at 8000 rpm, the obtained milk-white solid was washed thoroughly with deionized water to remove the residual acid, and finally dried at 80 ^{o}C in oven overnight. The synthesis milk-white solid were named as g-C$_3$N$_4$ NS.

Preparation of g-C$_3$N$_4$ NS/rGO$_x$ and g-C$_3$N$_4$ NS/rGO$_{20}$(M)

g-C$_3$N$_4$ NS/rGO$_x$ (x stand for the mass percentage ratio of rGO to g-C$_3$N$_4$ NS were prepared by the following method.[48] First, 100 mg GO was added to the 50 mL H$_2$O and the mixture solution was ultrasonicated for 1 h to obtain a homogeneous aqueous dispersion. Then, 500 mg g-C$_3$N$_4$ NS was added into the mixture and ultrasonicated for 30 min, and then the solution was stirred for 30 min at room temperature. Subsequently, the solution was sealed in a Teflon-lined autoclave and heated at 180 °C for 12 h, After cooling down naturally to room temperature, the obtained black product was collected by filtration, washed with distilled water, and freeze dried to obtain the g-C$_3$N$_4$ NS/rGO$_{20}$. g-C$_3$N$_4$/rGO$_{20}$, g-C$_3$N$_4$ NS/rGO$_{10}$

and g-C_3N_4 NS/rGO$_{30}$ were synthesized using the above procedure except that 500 mg bulk g-C_3N_4, 50 mg GO and 150 mg GO were added, respectively. In the process of hydrothermal reduction for synthesizing composite materials, water is used as reducing agent, and the preparation method is green and sustainable, which is better than other preparation methods[49, 50]. For comparison, g-C_3N_4 NS/rGO$_{20}$(M) was prepared by physical mixture of 100 mg rGO and 500 mg g-C_3N_4 NS.
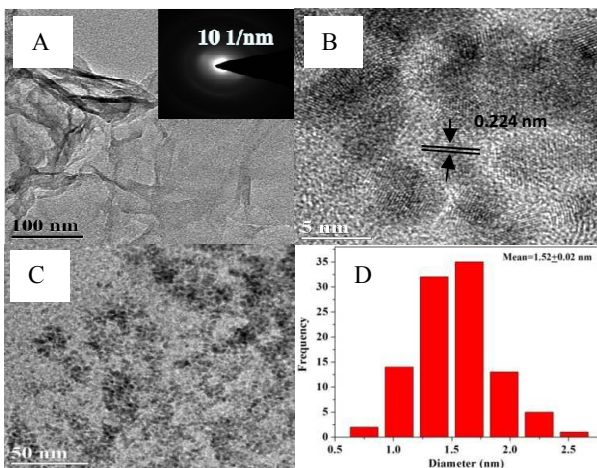

Fig. 1 TEM images of g-C_3N_4 NS/rGO$_{20}$ and their corresponding SAED patterns (inse (A, Pd-g-C_3N_4 NS/rGO$_{20}$ (B, C) and Pd particle-size distributionin the Pd-g-C_3N_4 NS/rGO$_{20}$ (D).

Preparation of supported Pd nanocatalysts

The supported Pd nanocatalysts were prepared by the impregnation method. Generally, 100 mg of catalyst support was dispersed into water (10 mL) by sonication. Then, 7.5 mL H_2PdCl_4 solution (2 mg·mL^{-1}) was added into the mixture and stirred overnight and 1 mol L^{-1} NaBH$_4$ (1 mL) was added dropwise to the suspension at 25 ^{o}C without the assistance of other stabilizers. After 2 h, the obtained mixture was separated by centrifugation and washed thoroughly with distilled water and ethanol, then dried at 60 ^{o}C for 6 h.

2.4 General procedure for the reduction of nitroarenes via the catalytic transfer hydrogenation reaction

In a typical catalytic transfer hydrogenation experiment, the Pd-g-C_3N_4 NS/rGO$_{20}$ (5 mg) and the alkenes compound (0.25 mmol) were well-mixed in 5 mL ethanol in a 25 mL round-bottom flask. Next, HCOONH$_4$ (2.5 mmol) and FA (2.5 mmol) were added into the resultant mixture and the reactions were stirred at 30 ^{o}C for a certain time. The advancement of the reaction was monitored by thin layered chromatography and GC. After accomplishment of the reaction, the catalyst was recovered by filtration and repeatedly washed by methanol for three times. Next, the catalysts were allowed to dry in a vacuum at 60 ^{o}C overnight for the further catalytic uses. The product was extracted with dichloromethane (3 ×10 mL) and dried over an anhydrous MgSO$_4$. The yield of the product was analyzed by GC.

3. Results and discussion

The nanostructures and morphologies of the as-prepared g-C_3N_4 NS/rGO$_{20}$ architectures were first examined by SEM and TEM. As shown in Fig.1, the TEM images clearly show the g-C_3N_4 NS/rGO$_{20}$ with the lamellar structures and a uniform nanosheet structure without obvious aggregation. The similar selected area electron diffraction (SAED) patterns (insets in Fig. 1A) of the g-C_3N_4 NS/rGO$_{20}$ demonstrate the homogeneous distribution of rGO sheets in the layered g-C_3N_4 structure, implying an ignorable effect of rGO modification on the layered structure of g-C_3N_4 NS.[51] As shown in Fig. 1C, fine Pd nanoparticles are uniformly distributed throughout the material. Besides, the high-resolution TEM image displays clear lattice fringes, suggesting good crystallinity. Fig. 1B shows the crystal plane spacing was measured as 0.224 nm, which is the (111) plane of face-centered cubic (fcc) Pd (0.224 nm).[52] The HRTEM observation indicates that the average size of Pd nanoparticles in the Pd-g-C_3N_4 NS/rGO$_{20}$ samples is approximately 1.52 nm on the basis of a count of more than 100 individual nanoparticles via TEM analysis (Fig. 1D). However, The Pd nanoparticles in the Pd-g-C_3N_4 NS possess an average particle size of 3.56 nm ± 0.02 nm (Fig. S1D, see Supporting Information), indicating that g-C_3N_4 NS coupling with rGO can effectively reduce the size of Pd nanoparticles, which is benefit for enhancing their catalytic performance.[53, 54] Furthermore, the detailed SEM morphology of a well-defined and interconnected 3D hierarchical structure can be clearly observed in the Fig. S1A and Fig. S1B. The content of Pd in the Pd-g-C_3N_4 NS/rGO$_{20}$ sample is determined by ICP-AES and amounted to 8.38 wt%.
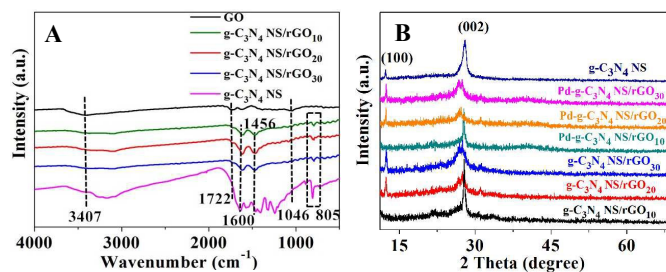

Fig. 2 FT-IR spectra of GO, g-C_3N_4 NS/rGO, g-C_3N_4 NS (A) and the XRD pattern of g-C_3N_4 NS, g-C_3N_4 NS/rGO, Pd-g-C_3N_4 NS/rGO (B).
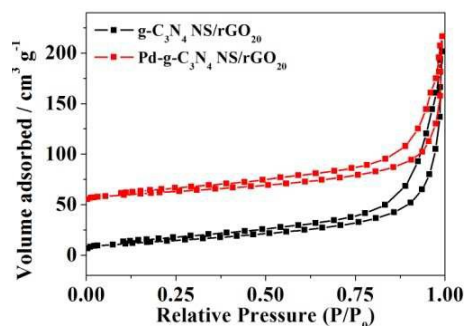
Fig. 3 The nitrogen adsorption-desorption isotherms of g-C_3N_4 NS/rGO$_{20}$, Pd-g-C_3N_4 NS/rGO$_{20}$.

ARTICLE   **Journal Name**

Fig. 2A shows the FTIR spectra of GO, g-C$_3$N$_4$ NS and g-C$_3$N$_4$ NS/rGO. The FTIR spectrum of GO showed the presence of polar oxygen-containing functionalities at 1046 (C-O-C stretching), 1722 (C=O stretching vibrations in carbonyl groups) and 3407 cm^{-1} (structural O-H groups). It is worthy of noting that the intensity of most of the oxygenated groups in the g-C$_3$N$_4$ NS/rGO significantly decreased or diminished after hydrothermal treatment, indicating that most of the oxygen functional groups in GO have been partially reduced. For g-C$_3$N$_4$ NS, several strong absorption bands in the range of 1200-1650 cm^{-1} was derived from the skeletal stretching of C-N heterocycles with peaks positioned at 1600 and 1456 cm^{-1}. The broad bands in the 3000-3700 cm^{-1} region can be assigned to N-H stretching vibration modes and the sharp band at 805 cm^{-1} was originated from the breathing vibration of tri-s-triazine units. All the g-C$_3$N$_4$ NS/rGO samples revealed almost similar characteristic features to the g-C$_3$N$_4$ NS, verifying that the structural integrity of g-C$_3$N$_4$ NS remained intact after the incorporation with rGO.

The structure of the as-prepared materials was characterized by XRD (Fig. 2B). The XRD patterns of g-C$_3$N$_4$ NS present a strong peak at 27.5°, which corresponds to the (002) crystallographic plane. The minor peaks (2θ = 13.1°) was indexed as (100) planes in-planar tris-s-triazine structural packing motifs. Besides, the weak diffraction peak of graphene at 2θ = 24.5° was shown due to the low content and fairly low diffraction intensity of rGO.[55] Fig. 2B shows no obvious difference in the composite material compared with g-C$_3$N$_4$ NS, which indicated g-C$_3$N$_4$ NS still retained in all g-C$_3$N$_4$ NS/rGO hybrids. No obvious Pd metal peaks can be observed, which can be ascribed to the well dispersion of Pd nanoparticles on g-C$_3$N$_4$ NS/rGO. As shown in Fig. 3, N$_2$ adsorption-desorption analysis indicated that g-C$_3$N$_4$ NS/rGO$_{20}$ hybrid with mesoporous and macroporous has a BET surface area of up to 49.8 m^2 g^{-1}, which nearly three times larger than that of g-C$_3$N$_4$ NS (14.2 m^2 g^{-1}) (Fig. S2A). This phenomenon can be assigned to the co-assembly of rGO and g-C$_3$N$_4$ NS, which form 3D architecture[56] and prevent the aggregation of g-C$_3$N$_4$ NS. Besides, it is found that g-C$_3$N$_4$ NS/rGO$_{20}$ exhibited higher specific surface area than g-C$_3$N$_4$ NS/rGO$_{10}$ (33.1 m^2 g^{-1}) and g-C$_3$N$_4$ NS/rGO$_{30}$ (24.9 m^2 g^{-1}) (Fig. S2B). Anyway, the high specific surface area of the g-C$_3$N$_4$ NS/rGO$_{20}$ is benefit for the well dispersion of Pd nanoparticles, absorbing more reactant molecules on the surface and providing more active species, which may lead to a better catalytic activity. The slight decreased surface area of Pd-g-C$_3$N$_4$ NS/rGO suggests the occupation of Pd nanoparticles inside the channel of g-C$_3$N$_4$ NS/rGO during the fabrication process (Fig. 3, Fig. S2B).

The X-ray photoelectron spectroscopy technique was further employed to evaluate the elemental composition and nitrogen content in g-C$_3$N$_4$ NS/rGO$_{20}$ nanocomposites. As shown in Fig. 4A, the Pd, N, C and O peaks are clearly observed. The Pd XPS of the catalyst demonstrates a double corresponding to Pd 3d$_{3/2}$ and Pd 3d$_{5/2}$ (Fig. 3B). The Pd 3d$_{5/2}$ peak and Pd 3d$_{3/2}$ peak at 338.1 eV 343 eV are related to Pd^{2+} (palladium oxide), while the Pd 3d$_{5/2}$ peak and Pd 3d$_{3/2}$ peak at 336.2 eV and 341.3 eV are attributed to Pd^0 (metallic palladium), which indicates metallic Pd as the major phase on the support.[57] The N 1s XPS spectra of g-C$_3$N$_4$ NS/rGO$_{20}$ can be fitted into three peaks (Fig. 4C) centred at 398.6, 399.9 and 401.5 eV, corresponding to sp^2 N atoms in triazine rings (N1), bridging N atoms in N-(C)3 (N2)[48] and amino functional groups (C-N-H)

(N3),[45] respectively. The C 1s peak of g-C$_3$N$_4$ NS/rGO composite can also be deconvoluted into three different components (Fig. 4D). The two main peaks located at 284.8 and 288.5 eV, corresponding to sp^2 C-C bonds (C1) and sp^2-bonded carbon in N-containing aromatic rings (N-C=N) (C3), respectively. The latter peak is supposed as the major carbon species of g-C$_3$N$_4$ NS.[45] The weak new peak at 286.4 eV is assigned to the carbon in C-N (C2). [58]
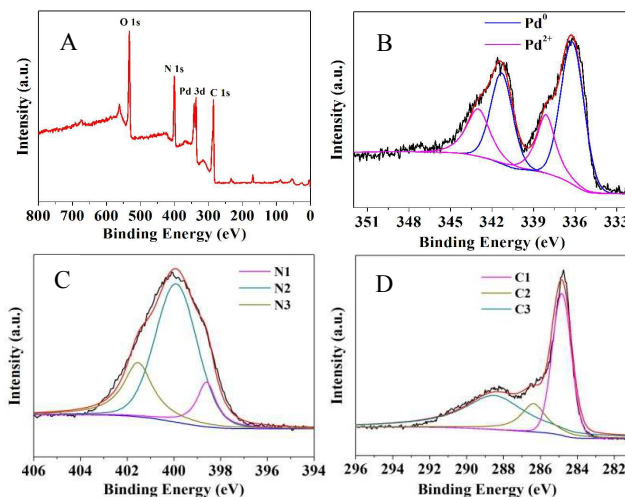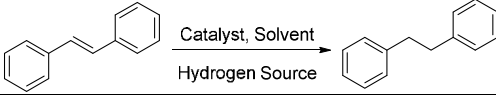

Fig. 4 XPS spectra of Pd-g-C$_3$N$_4$ NS/rGO$_{20}$ architectures (A), high-resolution Pd 3d (B), N 1s (C), and C 1s (D) in Pd-g-C$_3$N$_4$ NS/rGO$_{20}$.

To explore its potential applications, the Pd-g-C$_3$N$_4$ NS/rGO$_{20}$ composite has been employed for the hydrogenation reaction. Trans-stilbene was chosen as model substrate with the purpose of optimizing the reaction conditions. Blank experiments indicated that the reduction of trans-stilbene cannot proceed in the absence of hydrogen donors or a catalyst or Pd nanoparticles (Table 1, entries 1-3). To our surprise, the Pd-g-C$_3$N$_4$ NS/rGO$_{20}$ catalyst showed high catalytic activity toward the transfer hydrogenation of trans-stilbene with FA and HCOONH$_4$ as hydrogen donor at mild condition, achieving the highest turnover frequency (TOF) of 133 mol Pd mol^{-1} h^{-1} (Table 1, entries 4). A decrease in TOF values to 43 and 55 mol Pd mol^{-1} h^{-1} took place when FA:HCOONa and FA:HCOOK were used as the hydrogen donors (Table 1, entries 5-6). Besides, When FA and Et$_3$N were used as hydrogen source for the catalytic reduction of trans-stilbene (Table 1, entry 7); we achieved only 57% conversion after 1 h, which is very different with Zhao's work.[17] Various solvents were screened over Pd-g-C$_3$N$_4$ NS/rGO$_{20}$ (Table 1, entries 8-10) to test the solvent effect. The survey shows that methanol and THF provided the same outcome in the same condition, which is worse than ethanol (Table 1, entries 8, 9). Besides, DMF is a poor solvent for the catalytic transfer hydrogenation of trans-stilbene (Table 1, entry 10). So, ethanol was chosen for further studies as it is a more attractive solvent.[1] The effect of mass ratio of rGO in the catalyst on the hydrogenation of olefins was also investigated (Table 1, entries 4, 11-12). The optimal mass ratio of rGO in the nanocomposite was determined to be 20%. The reaction can be completed after 30 min catalyzed by Pd-g-C$_3$N$_4$ NS/rGO$_{20}$. The maximum TOF value of the reaction was estimated

Journal Name ARTICLE

to be 133 mol mol^{-1} Pd h^{-1}, surpassing majority heterogeneous catalysts using $N_2H_4 \cdot H_2O$, FA or i-PrOH as hydrogen source for hydrogenation of alkenes (Table S1). Furthermore, the Pd-g-C_3N_4 NS/rGO$_{20}$ (M) catalyst shows lower catalytic activity than Pd-g-C_3N_4 NS/rGO$_{20}$ composite (Table 1, entry 14). Therefore, it can be concluded that the improvement of the catalytic activity for Pd-g-C_3N_4 NS/rGO$_{20}$ is indeed attributed to synergistic effect between rGO and g-C_3N NS.[59] To better clarify the role of the support, we performed control experiments with commercial Pd@C. The Pd@C

provided 80% conversion after 1h, suggesting that our developed catalyst is superior to it. The phenomenon may come from the fact that our Pd-g-C_3N_4 NS/rGO catalysts can provide many more catalytic sites in comparison to this conventional Pd@C catalyst. Moreover, the component of the underlying material also plays a crucial role in determining the catalytic performance of the final materials. For comparison, Pd-g-C_3N_4 NS, Pd-bulk-g-C_3N_4/rGO$_{20}$ and Pd-rGO

Table 1 Reduction of alkene under various conditions. [a]

Entry	Catalysts	Hydrogen donors	Solvents	Time (h)	Conversion (%)	Selectivity (%)	TOF
1	-	FA:HCOONH$_4$	ethanol	3	-	-	-
2	g-C_3N_4 NS/rGO$_{20}$	FA:HCOONH$_4$	ethanol	3	-	-	-
3	Pd-g-C_3N_4 NS/rGO$_{20}$	-	ethanol	3	-	-	-
4	Pd-g-C_3N_4 NS/rGO$_{20}$	FA:HCOONH$_4$	ethanol	0.5	>99	>99	133
5	Pd-g-C_3N_4 NS/rGO$_{20}$	FA:HCOONa	ethanol	1	64	>99	43
6	Pd-g-C_3N_4 NS/rGO$_{20}$	FA:HCOOK	ethanol	1	82	>99	55
7[b]	Pd-g-C_3N_4 NS/rGO$_{20}$	FA:Et$_3$N	ethanol	1	57	>99	38
8	Pd-g-C_3N_4 NS/rGO$_{20}$	FA:HCOONH$_4$	methanol	2	78	>99	26
9	Pd-g-C_3N_4 NS/rGO$_{20}$	FA:HCOONH$_4$	THF	2	79	>99	26
10	Pd-g-C_3N_4 NS/rGO$_{20}$	FA:HCOONH$_4$	DMF	2	15	>99	5
11	Pd-g-C_3N_4 NS/rGO$_{10}$	FA:HCOONH$_4$	ethanol	1	87	100	58
12	Pd-g-C_3N_4 NS/rGO$_{30}$	FA:HCOONH$_4$	ethanol	1	100	98	65
13	Pd-bulk-g-C_3N_4/rGO$_{20}$	FA:HCOONH$_4$	ethanol	2	>99	100	33
14	Pd-g-C_3N_4 NS/rGO$_{20}$(M)	FA:HCOONH$_4$	ethanol	1	>99	100	66
15	Pd-g-C_3N_4 NS	FA:HCOONH$_4$	ethanol	1	>99	100	66
16	Pd-rGO	FA:HCOONH$_4$	ethanol	2	6	>99	2
17[c]	Pd@C	FA:HCOONH$_4$	ethanol	1	80	>99	53

[a] Reaction: *trans*-stilbene (0.25 mmol, 45 mg). Catalyst (5 mg, 1.5 mol% Pd). FA : Formate (2.5 mmol : 2.5 mmol). Solvent (5 mL), 30 °C. [b] FA : Et$_3$N (2.5 mmol : 2.5 mmol). [c] 1.5 mol% Pd.
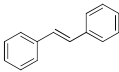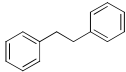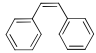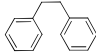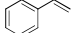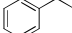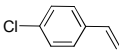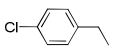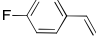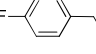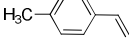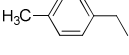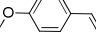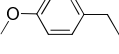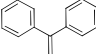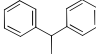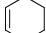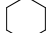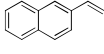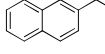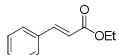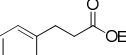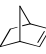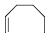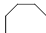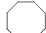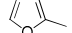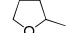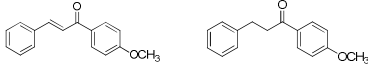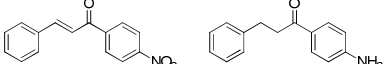
ARTICLE

were prepared. The transfer hydrogenation of alkene over Pd-bulk-g-C_3N_4/rGO$_{20}$, Pd-g-C_3N_4 NS and Pd-rGO were investigated under the same reaction conditions (Table 1, entries 13, 15-16). The full conversions of *trans*-stilbene catalyzed by Pd-bulk-g-C_3N_4/rGO$_{20}$ and Pd-g-C_3N_4 NS needed 2 h and 1 h, respectively. In addition, a low *trans*-stilbene conversion of 6% was produced after 2 h in the presence of the Pd-rGO catalyst, which shows that the introduction

of g-C_3N_4 NS could enhance the catalytic activity of rGO efficiently. It may be due to addition of carbon nitride nanosheets can effectively prevent the agglomeration of graphene.[60, 61] These results indicated that the nature of the support played important roles in the transfer hydrogenation of alkene reaction. The results further confirm the application potential of the hybrid materials in chemical synthesis.[31]
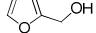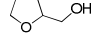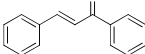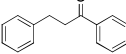
Table 2 Hydrogenation of various alkenes by using Pd-g-C_3N_4 NS/rGO$_{20}$ catalyst. [a]

Entry	Substrate	Product	Time (min)	Conversion (%)	Selectivity (%)	TOF
1			30	>99	>99	133
2			120	>99	>99	33
3			15	100	>99	266
4			30	97	57	74
5			30	100	>99	133
6			30	100	>99	133
7			30	100	>99	133
8			30	100	>99	133
9			30	100	>99	133
10			120	100	>99	33
11			30	98	>99	131
12			30	100	>99	133
13			240	86	>99	14
14[b]			90	100	>99	44
15			60	96	>99	64
16			60	94	>99	63
17			240	52	>99	9

Journal Name

ARTICLE

Entry	Substrate	Product	Time (min)	Conversion	Selectivity	TON
18[b]			30	100	>99	133
19[b]			45	>99	>99	89
20[b]			45	100	>99	89

[a] Reaction: 0.25 mmol Substrate. Pd-g-C_3N_4 NS/rGO$_{20}$ (5 mg, 1.5 mol% Pd). Ethanol. FA: HCOONH$_4$ (2.5 mmol : 2.5 mmol). 30 ^{o}C. [b] 50 ^{o}C.

Besides of high catalytic activity, the stability and reusability of the catalyst are also important issues for practical applications of unique structure catalysts in industry. We thus studied the catalytic performance of the used Pd-g-C_3N_4 NS/rGO$_{20}$ catalyst by considering *trans*-stilbene as the model substrate. The Pd-g-C_3N_4 NS/rGO$_{20}$ catalyst presented tremendous recyclability for at least 5 competitive catalytic cycles without significant loss of catalytic activity (Fig. 5A). After five recycled times, the catalyst gave corresponding 1,2-diphenylethane in 92% conversion at 30 min. Furthermore, the recovered catalyst was analyzed by FTIR, XRD, BET and TEM. As showed in Fig. S3, XRD and FTIR results showed that no obvious diffraction peak change can be observed between fresh and recycled catalyst, indicating good dispersion of metal and high durability and stability of the hybrid material. The results also coincide with the TEM images. The TEM images show that the Pd nanoparticles still exhibited a well-dispersed distribution over the support surface and no significant particle agglomeration (2.24 nm) (Fig. S3D). In addition, The BET surface area of the reused catalyst is 38 m^2 g^{-1}, which is comparable with the fresh catalyst. The preservation of BET surface area of the reused catalyst signifies high recyclability of the catalyst, revealing no sign of pore wall destruction and pores clogging (Fig. S3C). In order to further gain insight into the heterogeneous nature of the catalyst, the hot leaching test was carried out. After hydrogenation of *trans*-stilbene was run for 10 min, the Pd-g-C_3N_4 NS/rGO$_{20}$ catalyst was removed from the reaction mixture by centrifugation, and the filtrate was allowed to react for 2 h, negligible changes in conversion was observed (Fig. 5B). Obvious Pd leaching during the reaction was also excluded here according to the ICP result (data not shown), with the concentration of leached Pd species in the reaction solution below the detection limit of the equipment. Those finding demonstrated that Pd-g-C_3N_4 NS/rGO$_{20}$ exhibits typical heterogeneous catalyst nature. This high performance can be attributed to the strong synergistic effect between rGO and g-C_3N_4 NS. Those results illustrated that the composites can be thus considered as stable and reusable heterogeneous catalysts for practical applications.

We investigated the generality of the alkene hydrogenation reactions over Pd-g-C_3N_4 NS/rGO$_{20}$ with the optimized reaction parameters. In some cases, slight adjustment of the reaction conditions was required due to the distinct reactivity of reactants. As shown in Table 2, various unsaturated C=C bonds were successfully hydrogenated with good yield in ethanol at 30 ^{o}C. Successful hydrogenation was conducted for mono- and di-substituted alkenes
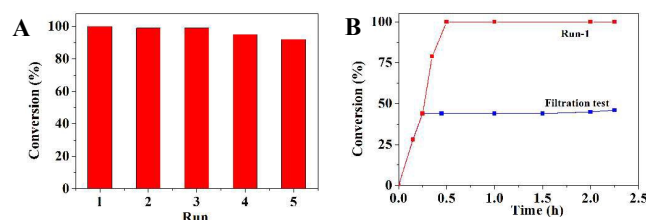

Fig. 5 Stability test for the transfer hydrogenation in the presence of Pd-g-C_3N_4 NS/rGO$_{20}$ catalyst (A) and the filtration test for the hydrogenation of alkene over Pd-g-C_3N_4 NS/rGO$_{20}$ (B).

(Table 2, entries 2, 8). The total conversion of styrene to ethylbenzene was achieved within 15 min (Table 2, entry 3). Interestingly, for the Cl-substituted styrene, slight dehalogenation process was observed during the reduction, which gave the products in 97% conversion and 57% selectivity (Table 2, entry 4). For F-substituted styrene, no dehalogenation process was observed during the reduction, which gave the product in 100% yield (Table 2, entry 5). The styrene compounds involving electron-rich groups such as p-methyl and p-methoxy were reduced to the corresponding products in an efficient fashion with absolute selectivity (Table 2, entries 6, 7). Cyclohexene and norbornylene, cyclic olefin, reached 100% product conversion after 30 min (Table 2, entries 9, 12). A vinyl substituted polycyclic aromatic hydrocarbon was reduced to the corresponding ethyl derivative with 100% conversion at 2 h (Table 2, entry 10). The hydrogenation of unsaturated C=C bonds was successfully achieved even in the presence of reducible substituent (ester group) (Table 2, entry 11). Surprisingly, very poor conversion was achieved for cyclooctene (Table 2, entry 13), which may be due to the presence of almost orthogonal allylic C-H bond.[17] When the reaction temperature rose to 50 ^{o}C, the cyclooctene conversion greatly increased and the reaction time for the hydrogenation of cyclooctene greatly decreased (Table 2, entry 14). The chemoselective transfer hydrogenation of C=C has been achieved for the α,β-unsaturated ketone, chalcone (Table 2, entry 18) with 100% conversion at 50 ^{o}C. What makes us happy is that 4-methoxychalcone and 4-nitrochalcone can gain excellent conversion under the same conditions (Table 2, entries 19-20). After knowing the excellent activity of the Pd-g-C_3N_4 NS/rGO$_{20}$ in reducing C=C bonds with FA and HCOONH$_4$, so we thus turned towards the hydrogenation of 2-methylfuran to 2-methyltetrahydrofuran and transfer hydrogenation 2-furanemethanol to 2-tetrahydrofurfuryl alcohol, which is the critical step for increasing the hydrogen/carbon

ARTICLE

Journal Name

ratios and thus transforming the biomass to renewable biofuel. The experimental results showed that the prepared catalyst has high catalytic performance for the hydrogenation of the two substances (Table 2, entries 15, 16).

4. Conclusion

In summary, we have demonstrated the successful fabrication of Pd-decorated architectures built from rGO and graphitic carbon nitride NS by means of a cost-effective and facile co-assembly approach. The hybrid composite showed high catalytic activity and stability in the alkene hydrogenation reactions with FA and AF as the hydrogen donors at mild conditions. The superior catalytic performance can be attributed to the synergistic effect between the highly dispersed Pd nanoparticles and the unique structure of the g-C_3N_4 NS/rGO$_{20}$ support, as well as the high specific surface area with high adsorption ability of the catalyst for the alkenes. We believe that this study could boost the feasibility of g-C_3N_4 NS/rGO as a supporter for integrating various functional metal particles for broader application field in organic synthesis under environmentally benign conditions.

5. Acknowledgments

References

1. L.-H. Gong, Y.-Y. Cai, X.-H. Li, Y.-N. Zhang, J. Su and J.-S. Chen, *Green Chem.*, 2014, **16**, 3746-3751.
2. Q. M. Kainz, R. Linhardt, R. N. Grass, G. Vilé, J. Pérez-Ramírez, W. J. Stark and O. Reiser, *Adv. Funct. Mater.*, 2014, **24**, 2020-2027.
3. K. Nomura, *J. Mol. Catal. A: Chem.*, 1998, **130**, 1-28.
4. V. K. Gupta, R. Jain, A. Mittal, T. A. Saleh, A. Nayak, S. Agarwal and S. Sikarwar, *Mater. Sci. Eng., C*, 2012, **32**, 12-17.
5. R. Saravanan, S. Karthikeyan, V. K. Gupta, G. Sekaran, V. Narayanan and A. Stephen, *Mater. Sci. Eng., C*, 2013, **33**, 91-98.
6. R. Saravanan, M. M. Khan, V. K. Gupta, E. Mosquera, F. Gracia, V. Narayanan and A. Stephen, *RSC Adv.*, 2015, **5**, 34645-34651.
7. C. K. Jain, *Int. J. Environ. Anal. Chem.*, 2004, **84**, 947-964.
8. I. Ali, Z. A. Alothman, A. Alwarthan, M. Asim and T. A. Khan, *Environ. Sci. Pollut. Res.*, 2014, **21**, 3218-3229.
9. I. Ali, Z. A. Al-Othman and A. Alwarthan, *J. Mol. Liq.*, 2016, **219**, 858-864.
10. I. Ali, Z. A. Al-Othman and A. Alwarthan, *J. Mol. Liq.*, 2016, **224**, 171-176.
11. I. Ali, Z. A. Alothman and M. M. Sanagi, *J. Mol. Liq.*, 2015, **211**, 457-465.
12. X. Bai, L. Wang, Y. Wang, W. Yao and Y. Zhu, *Appl. Catal., B*, 2014, **152-153**, 262-270.
13. A. Mittal, J. Mittal, A. Malviya and V. K. Gupta, *J. Colloid Interface Sci.*, 2010, **344**, 497-507.
14. V. K. Gupta, R. Jain, A. Nayak, S. Agarwal and M. Shrivastava, *Mater. Sci. Eng., C*, 2011, **31**, 1062-1067.
15. V. K. Gupta, S. Agarwal and T. A. Saleh, *J. Hazard. Mater.*, 2011, **185**, 17-23.
16. L. Qi and I. T. Horváth, *ACS Catal.*, 2012, **2**, 2247-2249.
17. J. Mondal, Q. T. Trinh, A. Jana, W. K. Ng, P. Borah, H. Hirao and Y. Zhao, *ACS Appl. Mater. Interfaces*, 2016, **8**, 15307-15319.
18. Z. S. Qureshi, P. B. Sarawade, M. Albert, V. D'Elia, M. N. Hedhili, K. Köhler and J.-M. Basset, *ChemCatChem*, 2015, **7**, 635-642.
19. C. Zhang, Y. Leng, P. Jiang, J. Li and S. Du, *ChemistrySelect*, 2017, **2**, 5469-5474.
20. V. K. Gupta and A. Nayak, *Chem. Eng. J.*, 2012, **180**, 81-90.
21. S. Karthikeyan, V. K. Gupta, R. Boopathy, A. Titus and G. Sekaran, *J. Mol. Liq.*, 2012, **173**, 153-163.
22. T. A. Saleh and V. K. Gupta, *J. Colloid Interface Sci.*, 2012, **371**, 101-106.
23. R. Saravanan, E. Thirumal, V. K. Gupta, V. Narayanan and A. Stephen, *J. Mol. Liq.*, 2013, **177**, 394-401.
24. M. Ghaedi, S. Hajjati, Z. Mahmudi, I. Tyagi, S. Agarwal, A. Maity and V. K. Gupta, *Chem. Eng. J.*, 2015, **268**, 28-37.
25. V. K. Gupta, A. Nayak, S. Agarwal and I. Tyagi, *J. Colloid Interface Sci.*, 2014, **417**, 420-430.
26. A. Mittal, J. Mittal, A. Malviya, D. Kaur and V. K. Gupta, *J. Colloid Interface Sci.*, 2010, **342**, 518-527.
27. A. Mittal, D. Kaur, A. Malviya, J. Mittal and V. K. Gupta, *J. Colloid Interface Sci.*, 2009, **337**, 345-354.
28. Y. Gong, M. Li, H. Li and Y. Wang, *Cheminform*, 2015, **17**, 715-736.
29. S. Cao, J. Low, J. Yu and M. Jaroniec, *Adv. Mater.*, 2015, **27**, 2150-2176.
30. P. Niu, L. Zhang, G. Liu and H.-M. Cheng, *Adv. Funct. Mater.*, 2012, **22**, 4763-4770.
31. R. Saravanan, N. Karthikeyan, V. K. Gupta, E. Thirumal, P. Thangadurai, V. Narayanan and A. Stephen, *Mater. Sci. Eng., C*, 2013, **33**, 2235-2244.
32. R. Saravanan, M. M. Khan, V. K. Gupta, E. Mosquera, F. Gracia, V. Narayanan and A. Stephen, *J. Colloid Interface Sci.*, 2015, **452**, 126-133.
33. R. Saravana, M. M. Khan, V. K. Gupta, E. E. M. Vargas, F. Gracia, V. Narayanan and S. Arumainathan, *RSC Adv.*, 2015, **5**, 34645-34651.
34. G. Liu, P. Niu, C. Sun, S. C. Smith, Z. Chen, G. Q. Lu and H. M. Cheng, *J. Am. Chem. Soc.*, 2010, **132**, 11642-11648.
35. L. Wang, C. Wang, X. Hu, H. Xue and H. Pang, *Chem. Asian. J.*, 2016, **11**, 3305-3328.
36. A. Asfaram, M. Ghaedi, S. Agarwal, I. Tyagi and V. Kumargupta, *RSC Adv.*, 2015, **5**, 18438-18450.
37. M. Hu, Z. Yao and X. Wang, *Ind. Eng. Chem. Res.*, 2017, **56**, 3477-3502.
38. D. Robati, B. Mirza, M. Rajabi, O. Moradi, I. Tyagi, S. Agarwal and V. K. Gupta, *Chem. Eng. J.*, 2016, **284**, 687-697.

Journal Name

ARTICLE

39. D. Robati, B. Mirza, M. Rajabi, O. Moradi, I. Tyagi, S. Agarwal and V. K. Gupta, *Chem. Eng. J.*, 2016, **284**, 687-697.

40. J. Yan, Z. Chen, H. Ji, Z. Liu, X. Wang, Y. Xu, X. She, L. Huang, L. Xu, H. Xu and H. Li, *Chemistry*, 2016, **22**, 4764-4773.

41. J. Oh, S. Lee, K. Zhang, J. O. Hwang, J. Han, G. Park, S. O. Kim, J. H. Park and S. Park, *Carbon*, 2014, **66**, 119-125.

42. W. B. Luo, S. L. Chou, J. Z. Wang, Y. C. Zhai and H. K. Liu, *Small*, 2015, **11**, 2817-2824.

43. W. J. Ong, L. L. Tan, S. P. Chai and S. T. Yong, *Chem. Commun.*, 2015, **51**, 858-861.

44. Y. Zhao, F. Zhao, X. Wang, C. Xu, Z. Zhang, G. Shi and L. Qu, *Angew. Chem. Int. Ed.*, 2014, **53**, 13934-13939.

45. K. Chen, Z. Chai, C. Li, L. Shi, M. Liu, Q. Xie, Y. Zhang, D. Xu, A. Manivannan and Z. Liu, *ACS Nano*, 2016, **10**, 3665-3673.

46. S. Yu, R. D. Webster, Y. Zhou and X. Yan, *Catal. Sci. Tech.*, 2017, **7**, 2050-2056.

47. Z. Zhou, J. Wang, J. Yu, Y. Shen, Y. Li, A. Liu, S. Liu and Y. Zhang, *J. Am. Chem. Soc.*, 2015, **137**, 2179-2182.

48. H. Huang, S. Yang, R. Vajtai, X. Wang and P. M. Ajayan, *Adv. Mater.*, 2014, **26**, 5160-5165.

49. G. Liao, S. Chen, X. Quan, H. Yu and H. Zhao, *J. Mater. Chem.*, 2012, **22**, 2721-2726.

50. J. Tian, R. Ning, Q. Liu, A. M. Asiri, A. O. Al-Youbi and X. Sun, *ACS Appl. Mater. Interfaces*, 2014, **6**, 1011-1017.

51. Y. Li, H. Zhang, P. Liu, D. Wang, Y. Li and H. Zhao, *Small*, 2013, **9**, 3336-3344.

52. Y. Xiong, J. M. McLellan, Y. Yin and Y. Xia, *Angew. Chem. Int. Ed.*, 2007, **46**, 790-794.

53. R. Saravanan, M. Mansoob Khan, V. K. Gupta, E. Mosquera, F. Gracia, V. Narayanan and A. Stephen, *J. Colloid Interface Sci.*, 2015, **452**, 126-133.

54. R. Saravanan, E. Thirumal, V. K. Gupta, V. Narayanan and A. Stephen, *J. Mol. Liq.*, 2013, **177**, 394-401.

55. Y. Wang, W. Wang, H. Mao, Y. Lu, J. Lu, J. Huang, Z. Ye and B. Lu, *ACS Appl. Mater. Interfaces*, 2014, **6**, 12698.

56. N. Senthilkumar, G. Gnana kumar and A. Manthiram, *Adv. Energy. Mater.*, 2018, **8**, 1702207.

57. S. Cheng, X. Meng, N. Shang, S. Gao, C. Feng, C. Wang and Z. Wang, *New J. Chem.*, 2017.

58. Q. Han, Z. Cheng, J. Gao, Y. Zhao, Z. Zhang, L. Dai and L. Qu, *Adv. Funct. Mater.*, 2017, **27**, 1606352.

59. X.-H. Li, J.-S. Chen, X. Wang, J. Sun and M. Antonietti, *J. Am. Chem. Soc.*, 2011, **133**, 8074-8077.

60. K. Ramachandran, T. Raj Kumar, K. J. Babu and G. Gnana Kumar, *Sci. Rep.*, 2016, **6**, 36583.

61. P. Vennila, J. Y. Dong, A. R. Kim and G. G. Kumar, *J. Alloys Compd.*, 2017, **703**, 633-642.

New Journal of Chemistry Accepted Manuscript

Pd anchored on C_3N_4 nanosheets/ reduced graphene oxide: an efficient catalyst for the transfer hydrogenation of alkenes

Jie Li[‡], Saisai Cheng[‡], Tianxing Du, Ningzhao Shang*, Shutao Gao, Cheng Feng,

Chun Wang*, Zhi Wang

College of Science, Hebei Agricultural University, Baoding 071001, China

Pd nanoparticles anchored on g-C_3N_4 NS/rGO was prepared by means of a cost-effective and facile co-assembly approach. The hybrid composite showed high catalytic activity and stability for the hydrogenation of alkenes with FA and $HCOONH_4$ as the hydrogen donors at mild conditions.